Batteries & Supercaps

Research Article
doi.org/10.1002/batt.202200464

Chemistry Europe
European Chemical Societies Publishing

www.batteries-supercaps.org

Evaluating the Polymer Backbone – Vinylene versus Styrene – of Anisyl-substituted Phenothiazines as Battery Electrode Materials

Gauthier Desmaizieres,[a] Verena Perner,[b] Daniel Wassy,[a] Martin Kolek,[b] Peter Bieker,*[b] Martin Winter,[b, c] and Birgit Esser*[a, d]

Organic electrode materials are capable candidates for next-generation greener energy storage solutions. One advantage is that their electrochemical performance can be tuned by structural modification. We herein investigate anisyl-substituted poly(vinyl-) and poly(styrylphenothiazines) as positive electrode materials for dual-ion batteries. π-Interactions – characteristic to phenothiazine redox polymers – are facilitated in the poly(styrene) derivatives **PSAPT** and **PSAPT-X-DVB** due to the longer spacing between phenothiazine units and polymer backbone and lead to high cycling stabilities, but reduce their specific capacities. In the poly(vinylenes), the linear **PVAPT** shows high cycling stability but a dissolution/redeposition mechanism, diminishing its capacity, while the cross-linked **X-PVAPT** demonstrates high cycling stabilities at specific capacities up to 81 mAh g^{-1} paired with an excellent rate performance, where 10,000 cycles at 100 C rate proceed with 86% capacity retention.

Introduction

The demand for electrically powered devices is continuously increasing. To satisfy the requirements of different applications and the needs for more sustainable and environmentally friendly energy storage solutions, new battery chemistries are required.[1–3] Organic electrode materials have been identified as a more sustainable alternative to traditional battery materials.[4,5] Their ability to be charged at high rates makes them attractive for high power applications,[6] and their processability and mechanically flexible nature – in particular of polymers – allows their use in flexible devices.[7,8] Many organic electrode materials have been developed with a range of specifications regarding specific capacity, rate capability and cycling stability.[9–15] Our groups focused on phenothiazine as p-type redox-active group,[16] as well as other researchers,[17–22] attractive for dual-ion[23,24] or anion-rocking chair batteries:[25] It has a relatively high redox potential of ca. 3.5 V vs. Li|Li$^+$; it can be incorporated into different polymeric architectures – as side group in aliphatic polymers or as part of the main chain in conjugated copolymers,[26,27] – and it has the unique ability to undergo π-(π-)interactions in its oxidized form with other neutral or oxidized phenothiazine units, which leads to a stabilization of the charged state, but can also reduce the accessible specific capacities.[28,29] This is in particular possible through the sulfur atom with diffuse orbitals and differentiates phenothiazine from its lower homologous phenoxazine, which does not undergo comparable π-(π-)interactions.[30] Particularly strong π-interactions were present in poly(3-vinyl-*N*-methylphenothiazine (**PVMPT**), enabled through a high polymer mobility in the employed electrolyte.[28] These resulted in an ultra-high cycling stability, however, paired with an unusual charge/discharge mechanism of dissolution and redeposition during charge and discharge of **PVMPT** and a reduction of the specific capacity to half of the theoretical value.[31] Cross-linking to **X-PVMPT**[32] or a change in electrolyte[33] reduced the solubility of the charged **(X-)PVMPT** and allowed accessing its full theoretical specific capacity. A change in polymer backbone to poly(norbornenes) diminished both solubility and π-interactions and furnished attractive battery polymers,[34] while attaching sterically demanding groups (e.g., mesityl) to the phenothiazine units in **PVMPT** resulted in a low cycling stability due to a complete lack of π-interactions combined with a high electrolyte solubility of the oxidized polymers.[35] Most of these polymers had in common that the nitrogen atom of the phenothiazine groups was substituted with methyl. Changing this substituent alters the redox properties of phenothiazine,

[a] *Dr. G. Desmaizieres, D. Wassy, Prof. Dr. B. Esser*
Institute of Organic Chemistry
University of Freiburg
Albertstraße 21, 79104 Freiburg (Germany)
[b] *V. Perner, Dr. M. Kolek, Dr. P. Bieker, Prof. Dr. M. Winter*
MEET Battery Research Center, Institute of Physical Chemistry
University of Münster
Corrensstr. 46, 48149 Münster (Germany)
E-mail: peter.bieker@uni-muenster.de
[c] *Prof. Dr. M. Winter*
Helmholtz-Institute Münster (HI MS)
IEK-12, Forschungszentrum Jülich GmbH, 48149 Münster (Germany)
[d] *Prof. Dr. B. Esser*
Current address: Institute of Organic Chemistry II and Advanced Materials
Ulm University
Albert-Einstein-Allee 11, 89081 Ulm (Germany)
E-mail: birgit.esser@uni-ulm.de
Homepage: http://www.esserlab.com

Supporting information for this article is available on the WWW under https://doi.org/10.1002/batt.202200464

Research Article
doi.org/10.1002/batt.202200464
Chemistry Europe
European Chemical Societies Publishing

where aryl groups can enhance the stability of the phenothiazine radical cation and thereby the reversibility of the redox process. *N*-aryl substituted phenothiazines as battery electrode materials have been reported before, but not with anisyl substitutents.[17–19,36,37] Anisyl as electron-rich aryl group is particularly well-suited, as we previously demonstrated in an investigation of conjugated phenothiazine copolymers.[26,27]

We herein investigate the influence of an anisyl substituent at the phenothiazine core on the redox properties, π-stacking ability and cycling behavior in poly(vinylene) and poly(styrene) derivatives. We show that the π-stacking ability is enhanced in the poly(styrene) derivatives **PSAPT** and **PSAPT-X-DVB** by a higher conformational flexibility of the phenothiazine units, obtained by introducing a longer linker between the PT units and the polymer backbone. This results in a high cycling stability, but diminishes their specific capacities to values significantly below the theoretical ones. In the poly(vinylenes) **PVAPT** and **X-PVAPT**, **PVAPT** shows a behavior reminiscent of **PVMPT** with a dissolution of the oxidized form in the electrolyte and a specific capacity of less than half of the theoretical value, while in cross-linked **X-PVAPT** by suppression of solubility and of conformational flexibility of the polymer side groups the full theoretical specific capacity can be accessed.

Results and Discussion

N-Anisylphenothiazine (**APT**) shows two reversible oxidation reactions at half-wave potentials of $E_{1/2} = 0.23$ and 1.04 V *vs.* $Fc|Fc^+$ in the cyclic voltammogram (CV) in solution (Figure 1 and Figure S22 for scan-rate dependent CV). Upon oxidation to the radical cation, its conformation changes from a butterfly shape with an angle of 155° (see X-ray structure in Figure 1) to a planar conformation. Additional conformational freedom exists in the rotation of the aryl substituent. Müller and co-workers recently studied the interplay of conformation and electronic properties in *N*-arylphenothiazines, including anisyl as aryl group.[38] Aryl substituents can assume an intra (quasi-equatorial) or extra (quasi-axial) conformation relative to the PT core. The intra conformation is energetically favorable for most aryl substituents except strongly electron-withdrawing ones. $\Delta\Delta G_{extra-intra}$ amounts to 3.3 kcal mol^{-1} (B3LYP/6-311++G**, PCM CH_2Cl_2) for **APT**, corresponding to 99.6% of the molecules assuming the intra conformation.[38] The molecular structure in the solid state of **APT** confirmed this prediction by showing the intra conformation (Figure 1). The intra preference for the oxidized, radical cation form of **APT** was also indicated from DFT calculations (Figure 1). The intra conformer of **APT$^{\bullet+}$** is by 7.8 kcal mol^{-1} more stable than the extra conformer (B3LYP-D3/def2-TZVP//PBEh-3c(COSMO acetonitrile)).

To investigate the conformational effect of strongly electron-withdrawing substituents, we synthesized and structurally characterized two PT derivatives with electron-withdrawing *N*-aryl substituents, namely with 4-(trifluoromethyl)phenyl (**CF3PT**) and 3,5-bis(trifluoromethyl)phenyl (**bCF3PT**, see Supporting Information). While the former assumed the intra conformation, the latter showed an extra conformation of the aryl substituent, caused by the stronger electron-withdrawing character of the aryl group bearing two CF_3 groups (see Supporting Information).

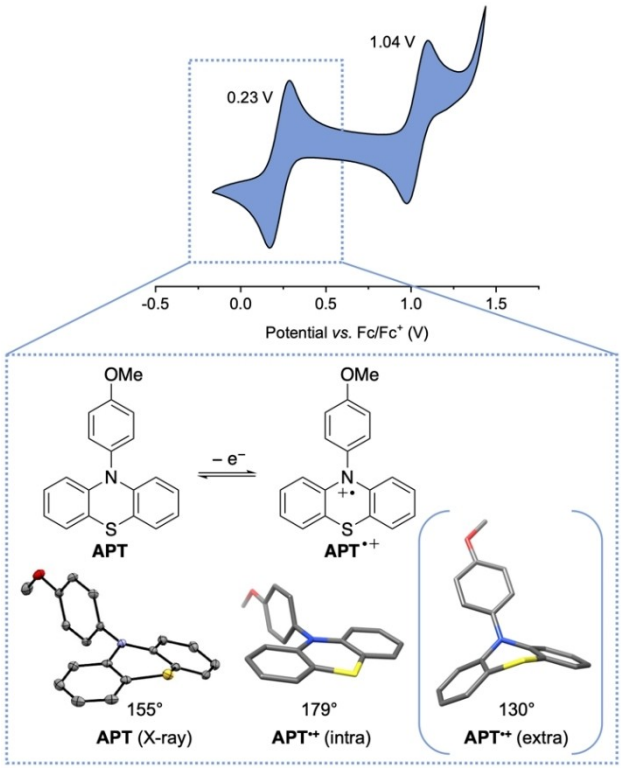

Figure 1. Cyclic voltammogram of *N*-anisylphenothiazine (**APT**) in solution (1 mM in CH_2Cl_2, 0.1 M *n*-Bu_4NPF_6, scan rate 0.1 V s^{-1}, glassy carbon electrode), redox reaction of **APT**, molecular structure in the solid state of **APT** with butterfly angle (displacement ellipsoids are shown at the 50% probability level; hydrogen atoms omitted for clarity) and calculated structures of the **APT** radical cation in intra and extra conformations with butterfly angles [PBEh-3c(COSMO acetonitrile)].

To obtain **APT** derivatives insoluble in battery electrolytes, we synthesized aliphatic polymers with **APT** as side group. As backbones, poly(vinylene) and a poly(styrene) were chosen. As shown in Scheme 1, the syntheses commenced from **APT**, synthesized as previously reported.[27] Vilsmeier-Haack formylation with DMF and $POCl_3$ to the aldehyde followed by Wittig reaction with the ylide generated in situ from methyltriphenylphosphonium bromide furnished *N*-anisyl-3-vinylphenothiazine (**1**) in 93% yield. The free-radical polymerization of **1**, initiated using AIBN, led to poly(3-vinyl-*N*-anisylphenothiazine) **PVAPT** in high yield of 84% with $M_n = 1.68 \times 10^4$ g mol^{-1} and a PDI of 2.7. Cross-linking can be required to obtain polymers insoluble in battery electrolytes – even in their oxidized form.[32] Hence we synthesized the **APT**-based cross-linker **2** by two-fold bromination of the PT core in **APT** followed by Suzuki-Miyaura coupling with vinylboronic acid pinacol ester in high yield of 84%. The co-polymerization of vinyl-APT **1** with 0.1 equiv. of divinyl-APT **2** furnished the cross-linked polymer **X-PVAPT** in 54% yield as insoluble material in common organic solvents.

For the poly(styrene) derivatives, monobrominated **APT** was required. The bromination of PT derivatives with 1 equiv. of

Research Article
doi.org/10.1002/batt.202200464
Chemistry Europe
European Chemical Societies Publishing

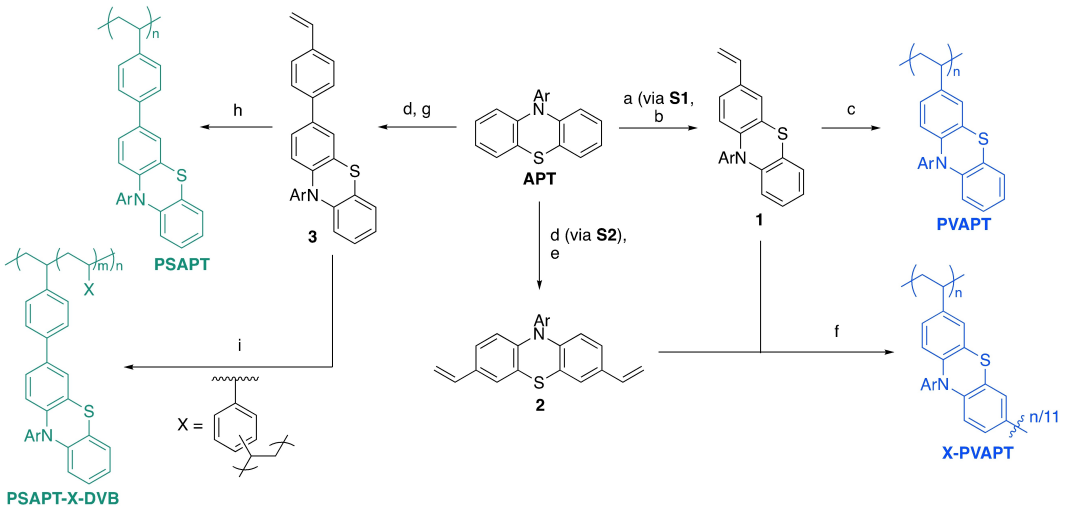

Scheme 1. Synthesis of **APT**-based polymers: a) $POCl_3$, DMF, 0 °C to 90 °C, 6 h, 97%; b) $MePPh_3Br$, KO*t*-Bu, THF, rt, 24 h, 96%; c) AIBN (2 mol%), toluene, 60 °C, 7 d, 84%; d) NBS, CH_2Cl_2, rt, 24 h, quant.; e) vinyl-B(pin), $Pd(PPh_3)_4$, NaOH, THF/H_2O, reflux, 4 h, 84%; f) **1** (1.0 equiv.), **2** (0.1 equiv.), AIBN (2 mol%), toluene, 60 °C, 2 d, 54%; g) 1. (i) *n*-BuLi, THF, −78 °C to rt, 30 min, (ii) MeOH, 2. Styryl-B(pin) (**S3**), $Pd(PPh_3)_4$, NaOH, THF/H_2O, 95 °C, 6 h, 85%; h) AIBN (2 mol%), THF, 70 °C, 15 h, 88%; i) Divinylbenzene (mixture of regioisomers, 0.1 equiv.), AIBN (5 mol%), THF, 70 °C, 17 h, 61%.

NBS typically affords mixtures of mono- and dibrominated PT in addition to unbrominated PT, which are difficult to separate by column chromatography. Hence APT was first brominated twice, and in the following step one of the bromides was changed back to H by bromo-lithium exchange and quenching with MeOH. This was followed by a Suzuki-Miyaura coupling with styrylboronic acid pinacol ester[15] to yield monomer **3** in excellent yield of 85%. The following free-radical polymerization afforded poly(3-styryl-*N*-anisylphenothiazine)) **PSAPT** in 88% yield as an insoluble polymer. Using 10 mol% AIBN, a soluble variant of **PSAPT** was also synthesized for CV and UV/Vis spectroscopic measurements in solution. To obtain a cross-linked derivative thereof, divinylbenzene (DVB) was chosen as cross-linker, and the polymerization of **3** in the presence of 0.1 equiv. of DVB led to **PSAPT-X-DVB** in 61% yield. NMR spectra of all soluble compounds can be found in Figures S1–S17.

All four polymers **PVAPT**, **X-PVAPT**, **PSAPT** or **PSAPT-X-DVB** showed high thermal stabilities with decomposition onset temperatures above 300 or 350 °C according to thermal gravimetric analyses (see Figures S18 and S19). The differential scanning calorimetric curves did not show clear events (Figures S20 and S21), indicative of the amorphous morphology of the polymers.

Both **PVAPT** and **PSAPT** showed two reversible redox processes in solution based on the oxidation of the APT side groups to radical cations and di-cations at all scan rates investigated (Figures 2, S23 and S24). For **PVAPT**, these were centered at half-wave potentials of $E_{1/2} = 0.17$ and 0.91 V *vs.* $Fc|Fc^+$, and for **PSAPT** at $E_{1/2} = 0.24$ and 0.88 V *vs.* $Fc|Fc^+$. Hence, in particular the second redox processes are shifted to lower potential compared to **APT** (0.23 and 1.04 V *vs.* $Fc|Fc^+$, see above), which might be due to the stabilization of the oxidized phenothiazine species in the polymers, i.e., through π-interactions. Plotting i_p vs. $v^{1/2}$ (v = scan rate) gave straight lines, indicative of reversible redox processes.

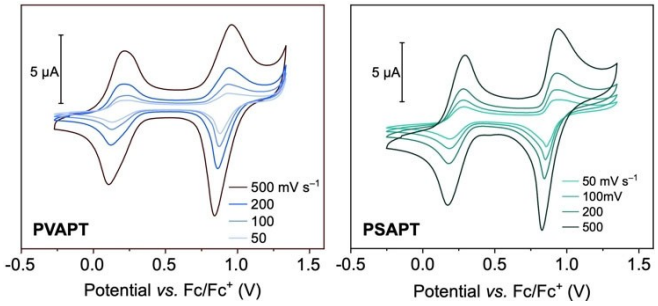

Figure 2. Cyclic voltammograms of **PVAPT** and **PSAPT** in solution at different scan rates (1 mM with respect to the redox-active subunit in CH_2Cl_2, 0.1 M *n*-Bu_4NPF_6, glassy carbon electrode).

To assess the electrochemical properties of the APT polymers in battery cells, we fabricated electrodes containing 50 wt% of the respective APT-polymer (**PVAPT**, **X-PVAPT**, **PSAPT** or **PSAPT-X-DVB**), 45 wt% carbon black as conductive additive and 5 wt% binder (PVdF).[39] Scanning electron microscopy (SEM) images of the electrodes can be found in the Supporting Information, Figures S39–S42. Metallic lithium was used as counter and reference electrode, and EC (ethylene carbonate)/DMC (dimethyl carbonate) 1:1 with 1 M $LiPF_6$ as typical[40] electrolyte to allow for best comparison with previous studies on PT-based polymers.[28,32,34] Using EC/EMC (ethyl methyl carbonate) 3:7 with 1 M $LiPF_6$, which was one of the best electrolyte for **PVMPT**-based electrodes,[33] did not lead to a better performance of the anisyl polymers discussed herein (selected electrochemical measurements in this electrolyte are shown in the Supporting Information, Figures S27, S29 and S31).

The CVs in composite electrodes show in each case a discrepancy between the first and the following cycles, namely

a shift to lower potential from the second cycle onwards (Figure 3A). This can be rationalized by an increase in electrical conductivity of the polymers upon partial oxidation. From the second cycle onwards, the half-wave potentials lie at similar values of 3.52–3.57 V *vs.* Li|Li$^+$ for all four polymers. What can further be noted is a decrease in specific current between cycle 2 and 18 for **PVAPT**. In previously investigated PT-based polymers this behavior was caused by the (partial) dissolution of the polymer in the electrolyte in its oxidized form.[31,33,35] This also happened for **PVAPT**, as the photograph of the separator taken from a cell after CV measurement in Figure 3A shows, which is pink/purple-colored due to the presence of oxidized **PVAPT**. Cross-linked **X-PVAPT** as well as **PSAPT** and **PSAPT-X-DVB**, on the other hand, remained insoluble in the electrolyte even in their oxidized form (see photographs of separators in the respective CVs in Figure 3A).

Scanning up to 4.5 V *vs.* Li|Li$^+$ allowed accessing the second redox processes of the polymers, however, they became irreversible after several cycles (see Figures S25, S26, S28 and S30). This we had also observed for all other PT-based polymers investigated in the past, and we ascribe this to irreversible side reactions of the dicationic PT units with carbonate solvent molecules. Hence only the first redox process of each polymer was further investigated.

The theoretical specific capacities of the polymers lie at 81 mAh g^{-1} for **PVAPT** and **X-PVAPT**, 66 mAh g^{-1} for **PSAPT** and 64 mAh g^{-1} for **PSAPT-X-DVB** for a one-electron oxidation of each APT unit. Constant current cycling measurements at 1 C rate provided initial specific discharge capacities of 39, 73 and 22 mAh g^{-1} for **PVAPT**, **X-PVAPT** and **PSAPT**, respectively, while for **PSAPT-X-DVB** after ten initial activation cycles 39 mAh g^{-1} were accessible (Figure 3B). After 1000 cycles at 1 C rate, the available specific capacities lay at 32, 71, 23 and 38 mAh g^{-1}, respectively, which in each case demonstrates an excellent cycling stability. The plot for **PVAPT** is strongly reminiscent of those of other PT-polymers that dissolved in the electrolyte during charge and (partially) redeposited on the positive electrode during discharge, visible in an initial decrease of the specific capacity during the first 40 cycles, and followed by a constant increase in the following cycles.[30,31,35] This dissolution in the charged state was also seen from UV/Vis spectra of the electrolyte extracted from the separator in the charged state (Figure S35), clearly showing bands for the oxidized polymer. In the discharged state, these bands disappeared, indicative of a (partial) deposition of the re-reduced polymer on the positive electrode. For the methyl derivative **PVMPT**, due to strong π-interactions between oxidized and neutral PT units, a stable film/deposit was formed during discharge of the "semi-oxidized" polymer, resulting in 50% of the theoretical specific capacity being accessible.[28,31] **PVAPT**, on the other hand, with its final specific capacity of 32 mAh g^{-1} after 1000 cycles, remained clearly below 50% of its theoretical value (50% would correspond to 41 mAh g^{-1} of theoretical specific capacity), which indicates that π-interactions played a less severe role in its discharge process, and the – after charge oxidized and dissolved – polymer could not as efficiently be redeposited during discharge (see SEM image in Figure S39).

X-PVAPT showed the best performance of all four polymers with an initial available specific discharge capacity of 73 mAh g^{-1} (90% of the theoretical value) that decreased by only 2% within 1000 cycles at 1 C rate. Hence cross-linking effectively inhibited dissolution of the polymer in its oxidized form, and **X-PVAPT** remained immobilized within the composite electrode during charge and discharge, as confirmed by

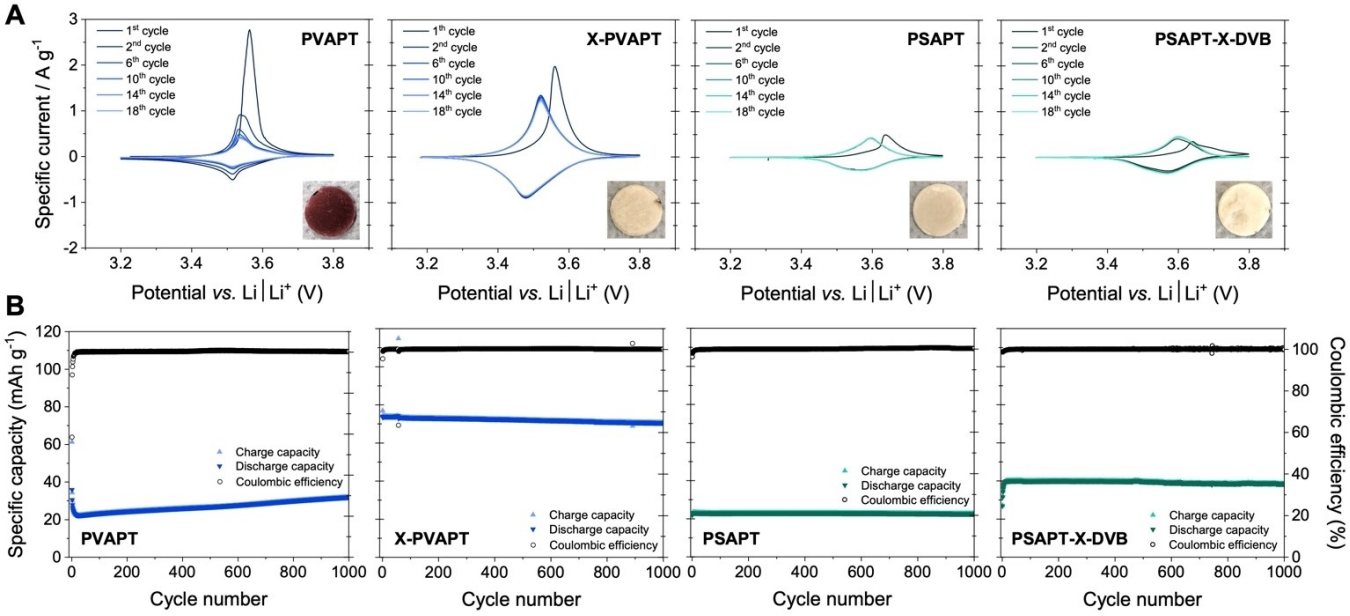

Figure 3. Electrochemical performance of the **APT**-based polymers in composite electrodes (**APT**-polymer/carbon black/PVdF (50:45:5 wt%), 1 M $LiPF_6$ in EC/DMC 1:1, counter/reference electrode: Li foil): A) cyclic voltammograms at a scan rate of 0.5 mV s^{-1} with photos of separators removed from cells of the CV measurement; B) constant current cycling at a 1 C rate.

Research Article
doi.org/10.1002/batt.202200464
Chemistry Europe
European Chemical Societies Publishing

UV/Vis spectra of electrolyte in the charged or discharged state (Figure S36). This cycling behavior is reminiscent of the cross-linked methyl-derivative **X-PVMPT**, which also showed excellent cycling stability at close to its theoretical specific capacity.[32] Hence **X-PVAPT** was further investigated regarding its rate capability and long-term cycling stability, as will be discussed below. The rate capability investigation for **PVAPT** can be found in the Supporting Information (Figure S32).

The styryl polymers **PSAPT** and **PSAPT-X-DVB** both demonstrated high cycling stability at 1 C rate, but at relatively low specific capacities. For **PSAPT**, the initial specific capacity of 22 mAh g^{-1} was held almost constant during 1000 cycles, while for **PSAPT-X-DVB** 38 mAh g^{-1} were accessible with a capacity retention of 97% after 1000 cycles. Both polymers remained insoluble in the electrolyte during cycling (see also photos of the separators taken from cycled cells in Figure 3A and UV/Vis spectra of the electrolyte of charged and discharged cells in Figures S37 and S38). Yet, it is interesting to note that in **PSAPT** only about half of the specific capacity of that in **PSAPT-X-DVB** was observed, which indicates that π-interactions might play a determining role in **PSAPT**, which can limit the specific capacity to half the expected value.[28,31] The rate capability investigations for **PSAPT** and **PSAPT-X-DVB** can be found in the Supporting Information (Figures S33 and S34).

Further proof for strong π-interactions at work in **PSAPT** compared to **PVAPT** were obtained from absorption spectroscopy measurements in solution and DFT calculations. The UV/Vis/NIR absorption spectra of oxidized samples of **PVAPT** and **PSAPT** (chemically oxidized using tris(4-bromophenyl)ammoniumyl hexachloroantimonate) showed several new bands compared to the neutral polymers (Figure 4A). Particularly relevant is the NIR band around 1500 nm, which stems from interactions of neutral **APT** units with **APT** radical cations, so called π-mers.[28,30] This band clearly appeared in oxidized **PSAPT** at 1482 nm, but not in oxidized **PVAPT**. In methyl-substituted **PVMPT**, a π-mer band had also occurred at 1485 nm, indicative of such π-interactions.[30] Hence in **PVAPT**, likely caused by the large size of the anisyl substituents, π-interactions are somewhat inhibited, while in **PSAPT**, the longer spacing to the poly(vinylene) backbone allows for π-interactions to form in spite of the bulky anisyl substituents.

Calculations on dimeric reference compounds for **PVAPT** and **PSAPT** show that in the radical cation state (one **APT** unit oxidized, one in the neutral state) π-interactions are facilitated with the styrene backbone (Figure 4B). The larger conformational flexibility allows for the **APT** units to assume a closer and more parallel orientation with an S–S distance of 3.58 Å (Figure 4B, bottom). Both **APT** units are planarized, which indicates that the positive charge is distributed over both units. In the vinyl case (top in Figure 4B), the distance between the **APT** units is larger (3.81 Å as closest N–S distance), and only one of the **APT** units assumes a planar conformation and likely accommodates most of the charge. Hence the longer spacing between **APT** units and polymer backbone in **PSAPT** enables the formation of substantial π-interactions, however, regarding battery performance, these interactions limit the available

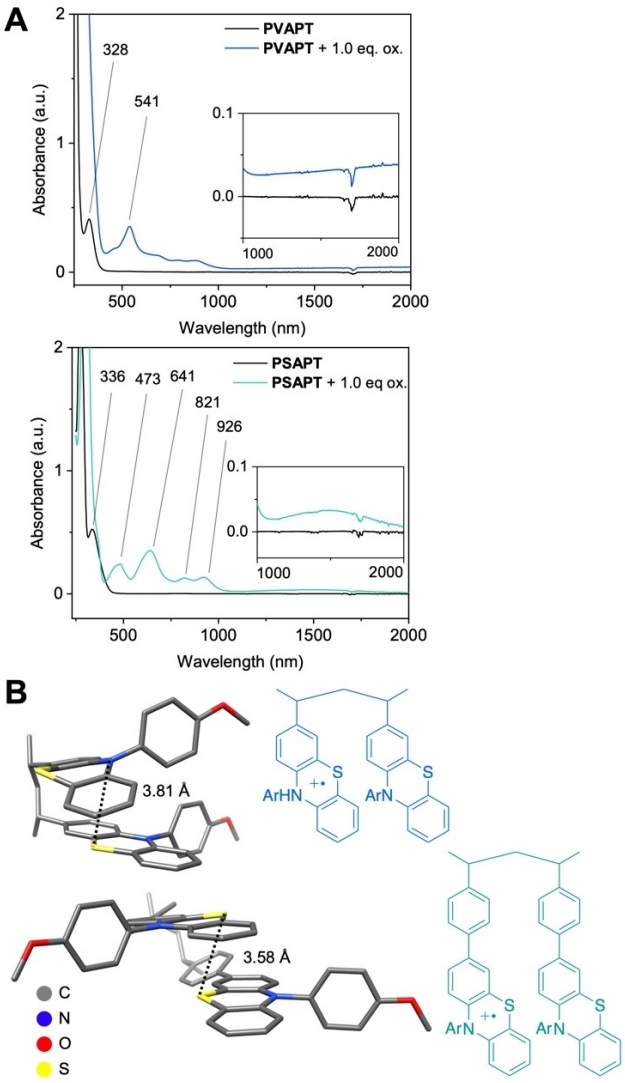

Figure 4. A) UV/vis/NIR spectra of **PVAPT** and **PSAPT** in CH_2Cl_2 in the neutral and oxidized state; B) Calculated structures of dimeric reference compounds for **PVAPT** and **PSAPT** in their singly oxidized (radical cation) form (PBEh-3c(COSMO acetonitrile)).

specific capacities to values significantly below the theoretical ones.

Due to its reversible redox activity and stable cycling behavior at a 1 C rate, we investigated **X-PVAPT** in more detail regarding its rate capability and long-term cycling stability. The C-rate test in Figure 5A demonstrates a strong rate performance, where even at a 100 C rate 69 mAh g^{-1} (85% of the theoretical specific capacity) were accessible. A long-term cycling test at 100 C rate (Figure 5B) showed an impressive stability. After 10,000 cycles, the capacity was measured to be 62 mAh g^{-1}, which corresponds to a capacity retention of 86% between cycles 6 and 10,000. Inspite of the fast charge/discharge rate, the differential specific capacity plot in Figure 5C shows a clear Faradaic redox activity and only a small voltage hysteresis of 60 mV between charge and discharge. Compared to methyl-substituted **X-PVMPT**, the rate capability of the anisyl derivative **X-PVAPT** is higher, albeit it has a lower

Research Article
doi.org/10.1002/batt.202200464

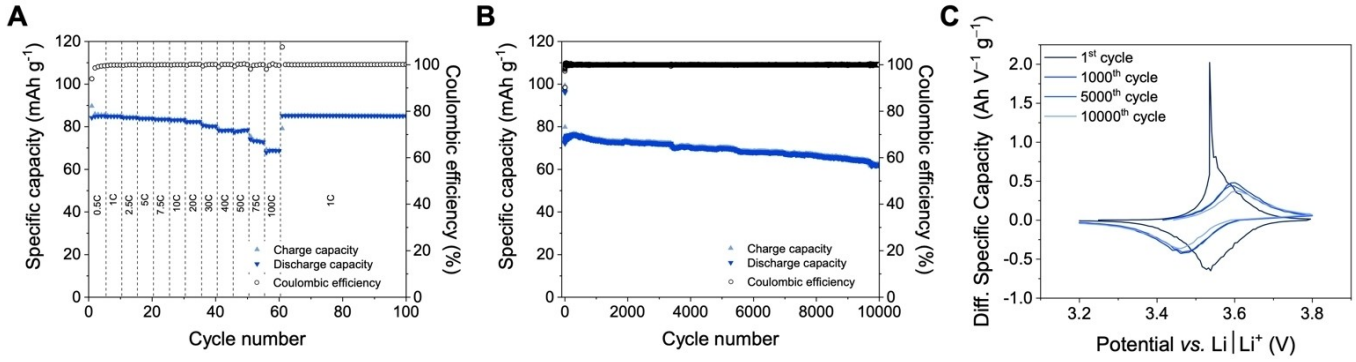

Figure 5. Rate performance of **X-PVAPT** in composite electrodes (**X-PVAPT**/carbon black/PVdF (50:45:5 wt%), 1 M $LiPF_6$ in EC/DMC 1:1, counter/reference electrode: Li foil): A) rate capability test; B) constant current cycling at a 100 C rate with C) differential specific capacity plots of selected cycles.

specific capacity.[32] Hence cross-linked **X-PVAPT** is a capable positive electrode material for high power applications in dual-ion or anion-rocking chair batteries.

Conclusion

In conclusion, we showed that anisyl substituents have a major effect on the electrochemical performance of aliphatic phenothiazine polymers. In the poly(styrene) derivatives **PSAPT** and **PSAPT-X-DVB**, π-Interactions – characteristic to phenothiazine redox polymers – are facilitated due to the longer spacing between phenothiazine units and polymer backbone. This furnished high cycling stabilities, however, also significantly reduced their specific capacities. Higher performance was obtained for the poly(vinylenes). The linear polymer **PVAPT** showed a high cycling stability but a dissolution/redeposition mechanism during charge/discharge, which diminished its capacity, while the cross-linked **X-PVAPT** demonstrated high cycling stabilities at specific capacities up to 81 mAh g^{-1} paired with an excellent rate performance, where 10,000 cycles at 100 C rate proceeded with 86% capacity retention. Our study demonstrates how the electrochemical performance of organic electrode materials can be tuned by simple modification of the molecular structure.

Experimental Section

Materials and methods

Air- and moisture-sensitive reactions were performed under an argon atmosphere using common Schlenk techniques in glassware heated *in vacuo* and flushed with argon several times. Anhydrous solvents were withdrawn from an SPS-unit from MB-SPS 800 System by M-Braun and stored over molecular sieves (3 Å). Ethyl acetate and cyclohexane were distilled prior to use. Commercially available chemicals were used without further purification. NMR spectra were recorded at room temperature on a *Bruker Avance III HD 500*, a *Bruker Avance II 400* or a *Bruker Avance III 300* spectrometer. Chemical shifts are reported in parts per million (ppm, δ scale). ^{1}H and ^{13}C spectra were calibrated against the residual proton and natural abundance ^{13}C resonances of $CDCl_3$ (^{1}H: 7.26 ppm, ^{13}C: 77.16 ppm) or against TMS (^{1}H, ^{13}C: 0 ppm). The following abbreviations were used: s = singlet, d = duplet, t = triplet, m = multiplet, br = broad. The coupling constants (*J*) are indicated in Hertz [Hz]. HR-MS spectra were measured on a THERMOFISHER SCIENTIFIC Exactive mass spectrometer with an orbitrap analyzer with atmospheric-pressure ionization (APCI) or electrospray ionization (ESI) as ionization methods. Thermal gravimetric analysis (TGA) measurements were performed on a STA 409 by NETZSCH and differential scanning calorimetry (DSC) measurements on a Seiko 6200 by SEIKO/PERKIN ELMER. Analytical gel permeation chromatography (GPC) was carried out with a *SECcurity* GPC System from Polymer Standards Service (PSS) using components of the 1260 *Infinity* series from Agilent Technologies (IsoPump: G1310B, auto sampler: ALS G1329B, UV-detector: MWD VL G1365D, RI-detector: RID G1362A) and a set of three columns (PSS SDV, 8 mm × 50 mm pre-column, 8 mm × 300 mm columns with a porosity of 1.000 Å and 100.000 Å). Stabilized THF with 2.5 ppm BHT at 35 °C was used as eluent with a flow rate of 1 mL min^{-1}, and calibration was performed using polystyrene standards by PSS. UV/Vis/NIR absorption spectra were measured with a *Lambda 950* spectrometer from PERKIN ELMER using sealable *Suprasil* quartz cuvettes (10 mm path length) from HELLMA ANALYTICS. UV/Vis measurements of electrolytes were performed on a *Cary 5000* spectrometer from AGILENT TECHNOLOGIES using quartz cuvettes from HELLMA ANALYTICS.

Single-crystal X-ray diffraction

The crystals were mounted on a MITIGEN holder in perfluoroether oil. XRD data were collected using a BRUKER SMART APEXII QUAZAR diffractometer equipped with an OXFORD Cryosystems 800 low-temperature device, operating at $T = 100$ K. Data were measured using ω and φ scans and MoKα radiation (microfocus sealed X-ray tube, 50 kV, 0.6 mA). The total number of runs and images was based on the strategy calculation by the BRUKER program APEX2. Cell parameters were retrieved using the SAINT[41] software and refined using SAINT Data reduction was performed using the SAINT[41] software, which corrects for Lorentz polarization (SAINT V8.37A, Bruker AXS, Madison, Wisconsin, USA, **2015**).

Cyclic voltammetry in solution

Cyclic voltammetry measurements were performed in solution inside a glovebox using an Autolab PGSTAT 128N by Metrohm. As working electrode, a glassy carbon electrode (2 mm diameter) were used. A platinum rod served as counter electrode, and as reference electrode an Ag/$AgNO_3$ electrode containing a silver wire immersed in an inner chamber filled with 0.1 M $AgNO_3$ and containing 0.1 M *n*-

Bu_4NPF_6 was used. The analyte concentration was 1 mM in CH_2Cl_2, for the polymers the concentration is given with respect to the redox-active subunit. As internal reference, the Fc/Fc^+ redox couple was used.

Electrode preparation

The fabrication of composite electrodes of **PVAPT**, **X-PVAPT**, **PSAPT** and **PSAPT-X-DVB** was performed in a dry room with less than 0.02% moisture. Composite electrodes were prepared using 50 wt% of the respective polymer, 45 wt% carbon black (Super C65, IMERYS), and 5 wt% binder (poly(vinylidene difluoride) (PVdF), KYNARFLEX 761a, ARKEMA). The polymer was pre-dried in a BÜCHI B-585 glass oven under reduced pressure (10^{-3} mbar) at 60 °C for 1 day. Dry mixtures of the polymer, carbon black, and binder were dispersed in NMP (1-methyl-2-pyrrolidinone, 99.5%, ACROS Organics, stored over molecular sieve) until a honey-like viscosity was obtained. The electrode formulations were stirred at 20 °C for 1 day. The resulting paste was blade-coated onto KOH-etched aluminum foil (Goodfellow, >99.8%; etched by immersion at 20 °C for 45 s in 3 M aq. KOH solution). A micrometer-adjustable film applicator (Hohsen Corp.) with blade-to-substrate gap (wet film thickness) of 50 μm at 50 mm s^{-1} was used. The coated aluminum foil was dried at 80 °C for 30 min, and electrodes with a diameter of 12 mm were punched out with a handheld electrode-punching device (HOHSEN CORP.). Electrodes were dried at 60 °C under reduced pressure (10^{-3} mbar) for 1 day before electrochemical cell assembly. The resulting electrodes showed a dry film thickness of 3–6 μm when subtracting the thickness of the current collector (20 μm). The mass loadings amounted to values between 0.10 and 0.23 mg cm^{-2}.

Electrochemical characterization of composite electrodes

Cells were assembled in a dry room with less than 20 ppm moisture. Electrochemical measurements were performed in a three-electrode setup using Swagelok® T-cells. Lithium foil (Albemarle, battery grade, 500 μm) was used as counter (ø = 12 mm) and reference (ø = 5 mm) electrode. The investigated polymers were used as active material in the working electrode. Between the electrodes six layers of Freudenberg 2190 non-woven poly(propylene) separators (ø = 13 mm) soaked with electrolyte (1 M $LiPF_6$ in EC : DMC 1 : 1 by weight, BASF *Selectilyte*) were placed (ø = 13 mm and 130 μL electrolyte between counter and working electrode, ø = 10 mm and 60 μL electrolyte at reference electrode). Cyclic voltammetry (CV) measurements were performed on a VMP3 potentiostat (BioLogic Science Instruments) at a scan rate of 500 μV s^{-1}. Constant current cycling (CC) investigations were carried out on a MACCOR 4000series battery cycler. The various conditions are stated in the respective figure caption. All electrochemical measurements on battery cells were conducted in climatic chambers (Binder GmbH, Germany) at 20 °C. The capacities mentioned herein were calculated for the amount of active material and are therefore displayed as specific values.

Synthetic manipulations

10-(4-(trifluoromethyl)phenyl)-10*H*-phenothiazine (CF3PT). A solution of phenothiazine (**PT**, 2.00 g, 15.5 mmol), potassium *tert*-butoxide (2.08 g, 18.6 mmol), Pd_2dba_3 (270 mg, 295 μmol), tricyclohexylphosphine (174 mg, 0.62 mmol) and 1-bromo-4-(trifluoromethyl)benzene (3.48 g, 15.5 mmol) in degassed anhydrous toluene (20 mL) was purged for 15 min with argon and stirred under reflux for 24 h. The reaction mixture was cooled to room temperature and water (20 mL) was added. The aqueous phase was extracted with EtOAc (3 × 50 mL). The combined organic layers were dried ($MgSO_4$), filtered, and the solvent was evaporated under vacuum. Column chromatography (silica gel, cyclohexane) followed by recrystallization in 2-propanol afforded **CF3PT** (3.98 g, 11.6 mmol, 75%) as a white solid. ^{1}H NMR (500 MHz, $CDCl_3$) δ 7.68 (d, J = 8.4 Hz, 1H), 7.34 (d, J = 8.3 Hz, 1H), 7.09–7.05 (m, 1H), 7.00 (td, J = 7.5, 1.3 Hz, 1H), 6.68 (dd, J = 8.1, 1.3 Hz, 1H); ^{13}C NMR (126 MHz, $CDCl_3$) δ 146.3, 142.8, 127.8, 127.4, 127.4, 127.4, 127.3, 127.2, 126.5, 124.6, 124.4, 120.8; HRMS (ESI+): *m/z* calcd. for $C_{19}H_{12}F_3NS$ 343.0637 $[M]^+$, found 343.0637.

10-(3,5-Bis(trifluoromethyl)phenyl)-10*H*-phenothiazine (bCF3PT). A solution of phenothiazine (**PT**, 130 mg, 1.01 mmol), potassium *tert*-butoxide (124 mg, 1.11 mmol), $Pd(OAc)_2$ (11 mg, 50 μmol), RuPhos (19 mg, 41 μmol) and 1-bromo-3,5-bis(trifluoromethyl)benzene (264 mg, 0.90 mmol) in degassed anhydrous 1,4-dioxane (6 mL) was purged for 15 min with argon and stirred under reflux for 24 h. The reaction mixture was cooled to room temperature and water (20 mL) was added. The aqueous phase was extracted with EtOAc (3 × 20 mL). The combined organic layers were dried ($MgSO_4$), filtered, and the solvent was evaporated under vacuum. Column chromatography (silica gel, cyclohexane) followed by recrystallization from 2-propanol afforded **bCF3PT** (248 mg, 0.61 mmol, 81%) as a white solid. ^{1}H NMR (500 MHz, Chloroform-*d*) δ 7.59 (s, 1H), 7.55 (s, 2H), 7.37 (dd, J = 7.7, 1.5 Hz, 2H), 7.23 (ddd, J = 7.9, 7.4, 1.6 Hz, 2H), 7.14 (td, J = 7.6, 1.3 Hz, 2H), 6.96 (dd, J = 8.0, 1.3 Hz, 2H); ^{13}C NMR (126 MHz, $CDCl_3$) δ 145.9, 141.6, 133.1, 132.8, 130.1, 128.7, 127.6, 125.7, 123.2, 120.5, 116.9; HRMS (ESI+): *m/z* calcd. for $C_{20}H_{11}F_6NS$ 411.0511 $[M]^+$; found 411.0520.

10-(4-Methoxyphenyl)-10H-phenothiazine (APT). A solution of phenothiazine (**PT**, 1.02 g, 7.97 mmol), sodium *tert*-butoxide (1.20 g, 12.5 mmol), Pd_2dba_3 (366 mg, 400 μmol), tricyclohexylphosphine (157 mg, 560 μmol) and 1-bromo-4-methoxybenzene (1 mL, 7.97 mmol) in degassed toluene (20 mL) was purged for 15 min with argon and stirred under reflux for 24 h. The reaction mixture was cooled to room temperature and water (20 mL) was added. The aqueous phase was extracted with EtOAc (3 × 50 mL). The combined organic layers were dried ($MgSO_4$), filtered, and the solvent was evaporated under vacuum. Column chromatography (silica gel, cyclohexane) followed by recrystallization from EtOAc afforded **APT** (1.81 g, 5.90 mmol, 74%) as brown crystals. ^{1}H NMR (300 MHz, CD_2Cl_2) δ 7.33–7.27 (m, 2H), 7.15–7.10 (m, 2H), 6.98 (dd, J = 7.1, 2.0 Hz, 2H), 6.87–6.75 (m, 2H), 6.22–6.18 (m, 2H), 6.20–6.16 (m, 2H), 3.89 (s, 3H); ^{13}C NMR (101 MHz, CD_2Cl_2) δ 159.3, 144.7, 133.4, 132.3, 126.9, 126.7, 122.3, 119.8, 116.0, 115.7, 55.6; HRMS (ESI+): *m/z* calcd. for $C_{19}H_{15}NOS$ 305.0874 $[M]^+$, found 305.0869.

10-(4-Methoxyphenyl)-10*H*-phenothiazine-3-carbaldehyde (S1). Phosphoryl chloride (0.18 mL, 1.97 mmol) was added dropwise to a solution of 10-(4-methoxyphenyl)-10*H*-phenothiazine (**APT**, 500 mg, 1.94 mmol) in a mixture of DMF (0.60 mL) and 1,2-dichloroethane (2 mL) at 0 °C, and the reaction mixture was stirred at 90 °C for 22 h afterwards. The solution was cooled to rt, and saturated aq. NaOAc was added. The aqueous layer was extracted with EtOAc (3 × 50 mL). The combined organic layers were dried over $MgSO_4$, filtered and evaporated to dryness under reduced pressure. Column chromatography (silica gel, ethyl acetate) afforded **S1** (528 mg, 1.58 mmol, 97%) as an orange solid. ^{1}H NMR (400 MHz, $CDCl_3$) δ 9.69 (s, 1H), 7.45 (d, J = 1.9 Hz, 1H), 7.32–7.24 (m, 3H), 7.18–7.09 (m, 2H), 7.00–6.91 (m, 1H), 6.88–6.78 (m, 2H), 6.20 (d, J = 8.6 Hz, 1H), 6.19–6.12 (m, 1H), 3.91 (s, 3H); ^{13}C NMR (126 MHz, $CDCl_3$) δ 189.8, 159.7, 149.6, 142.9, 132.4, 131.8, 131.0, 130.0, 127.5, 127.2, 126.7, 123.6, 120.1, 119.1, 116.5, 116.3, 115.1, 55.7; HRMS (ESI+): *m/z* calcd. for $C_{20}H_{16}NO_2S$ 334.0902 $[M+H]^+$; found 334.0895.

10-(4-Methoxyphenyl)-3-vinyl-10*H*-phenothiazine (1). 10-(4-Methoxyphenyl)-10*H*-phenothiazine-3-carbaldehyde (**S1**, 800 mg, 2.40 mmol) was added to a suspension of potassium *tert*-butoxide

(500 mg, 4.46 mmol) and methyltriphenylphosphonium bromide (1.30 g, 3.64 mmol) in THF (6 mL). The mixture was stirred at room temperature for 24 h. H_2O was added, and the aqueous layer was extracted with ethyl acetate (3×75 mL). The combined organic layers were dried over $MgSO_4$, filtered and evaporated to dryness under reduced pressure. Column chromatography (silica gel, cyclohexane/EtOAc: 50/1 + 5 mol% Et_3N) afforded **1** (765 mg, 2.29 mmol, 96%) as a yellow oil. ^{1}H NMR (400 MHz, $CDCl_3$) δ 7.33–7.27 (m, 2H), 7.14–7.09 (m, 2H), 7.07 (d, J = 2.3 Hz, 1H), 7.01–6.98 (m, 1H), 6.87–6.76 (m, 3H), 6.52 (dd, J = 17.6, 10.9 Hz, 1H), 6.20 (m, 1H), 6.12 (d, J = 8.5 Hz, 1H), 5.55 (dd, J = 17.6, 0.9 Hz, 1H), 5.10(dd, J = 10.9, 0.9 Hz, 1H), 3.89 (s, 3H); ^{13}C NMR (101 MHz, $CDCl_3$) δ 159.4, 144.3, 135.4, 133.3, 132.3, 132.2, 126.9, 126.7, 125.1, 124.1, 122.4, 122.3, 119.7, 119.3, 116.0, 115.7, 115.5, 112.0, 55.6; HRMS (ESI+): *m/z* calcd. for $C_{21}H_{17}NOS$ 331.1031 $[M]^+$, found 331.1028.

Poly(10-(4-methoxyphenyl)-3-vinyl-10*H*-phenothiazine) (PVAPT). 10-(4-Methoxyphenyl)-3-vinyl-10*H*-phenothiazine (**1**, 570 mg, 1.7 mmol) was dissolved in anhydrous toluene (1.5 mL) and cooled for 5 min to −10 °C. A solution of AIBN (6.0 mg, 34.0 μmol, 2 mol%) in anhydrous toluene (0.5 mL) was added, and the reaction was placed in a preheated oil bath at 60 °C for 7 d. The resulting yellow suspension was poured into methanol. Dissolution in chloroform (2×0.5 mL) and consequent precipitation from methanol (2× 200 mL) and cyclohexane (200 mL) afforded **PVAPT** (456 mg, 84%) as a white solid. ^{1}H NMR (300 MHz, $CDCl_3$) δ 7.21–6.97 (m, 2H), 6.96–6.51 (m, 5H), 6.33–5.73 (m, 4H) 3.85–3,58 (m, 3H), 1.41–0.89 (m, 3H); GPC (eluent THF, polystyrene standard): $M_n = 1.73 \times 10^4$ g/mol, M_w/M_n 5.02; TGA (10 °C/min, N_2): $T_{d10\%} = 379$ °C.

3,7-Dibromo-10-(4-methoxyphenyl)-10*H*-phenothiazine (S2). 10-(4-Methoxyphenyl)-10*H*-phenothiazine (**APT**, 300 mg, 0.98 mmol) was dissolved in CH_2Cl_2 and cooled at 0 °C. *N*-Bromosuccinimide (370 mg, 2.08 mmol) was added, and the reaction was allowed to stir at room temperature for 24 h. H_2O was added and the aqueous layer was extracted with CH_2Cl_2 (3×75 mL). The combined organic layers were washed with brine, dried over $MgSO_4$, filtered and evaporated to dryness. Column chromatography (silica gel, CH_2Cl_2) afforded **S2** (441 mg, 97%) as an orange solid. ^{1}H NMR (400 MHz, $CDCl_3$) δ 7.26–7.22 (m, 2H), 7.13–7.08 (m, 2H), 7.07 (d, J = 2.3 Hz, 2H), 6.90 (dd, J = 8.8, 2.3 Hz, 2H), 6.01 (d, J = 8.8 Hz, 2H) 3.89 (s, 3H); ^{13}C NMR (101 MHz, $CDCl_3$) δ 159.7, 143.6, 132.6, 131.9, 129.8, 128.8, 121.2, 117.0, 116.3, 114.6, 55.7; HRMS (APCI+): *m/z* calcd. for $C_{19}H_{13}{}^{79}Br^{81}BrNOS$ 462.9059 $[M]^{\bullet+}$, found 462.9059.

10-(4-Methoxyphenyl)-3,7-divinyl-10*H*-phenothiazine (2). A mixture of 3,7-dibromo-10-(4-methoxyphenyl)-10*H*-phenothiazine (**S2**, 100 mg, 0.22 mmol), 4,4,5,5-tetramethyl-2-vinyl-1,3,2-dioxaborolane (vinyl-B(pin), 0.17 mL, 0.99 mmol) and $Pd(PPh_3)_4$ (15 mg, 130 μmol, 6 mol%) in a degassed mixture of THF (5 mL) and aq. NaOH (10% w/w, 1.2 mL) was heated to 90 °C for 4 h. The reaction was cooled to room temperature, H_2O was added, and the aqueous layer was extracted with dichloromethane (3×25 mL). The combined organic layers were dried over $MgSO_4$, filtered and evaporated to dryness. Column chromatography (silica gel, cyclohexane/EtOAc: 50/1 to 20/1 with 5 mol% Et_3N) afforded **2** (77 mg, quant.) as an orange solid. ^{1}H NMR (400 MHz, $CDCl_3$) δ 7.22–7.18 (m, 2H), 7.05–7.01 (m, 2H), 6.96 (d, J = 2.1 Hz, 2H), 6.76 (dd, J = 8.6, 2.1 Hz, 2H), 6.43 (dd, J = 17.6, 10.9 Hz, 2H), 6.01 (d, J = 8.6 Hz, 2H), 5.46 (dd, J = 17.6, 0.9 Hz, 2H), 5.01 (dd, J = 10.9, 0.9 Hz, 2H), 3.82 (s, 3H); ^{13}C NMR (101 MHz, $CDCl_3$) δ 159.5, 143.8, 135.4, 133.3, 132.2, 132.1, 125.1, 124.1, 119.4, 116.1, 115.6, 112.1, 55.6; HRMS (ESI+): *m/z* calcd. for $C_{23}H_{19}NOS$ 357.1187 $[M]^+$, found 357.1183.

Cross-linked poly(10-(4-methoxyphenyl)-3-vinyl-10H-phenothiazine) (X-PVAPT). A solution of 10-(4-methoxyphenyl)-3-vinyl-10*H*-phenothiazine (**1**, 570 mg, 1.72 mmol), 10-(4-methoxyphenyl)-3,7-divinyl-10*H*-phenothiazine (**2**, 68 mg, 0.19 mmol, 11 mol%) and AIBN (6 mg, 34 μmol, 2 mol%) in anhydrous toluene (2 mL) was placed in a preheated oil bath and stirred at 60 °C for 2 d. The reaction was cooled to room temperature and MeOH was added to quench the reaction. After evaporation, the polymer was SOXHLET-extracted with MeOH, EtOAc, acetone and CH_2Cl_2 to afford **X-PVAPT** (305 mg, 54%) as a yellow solid. TGA (10 °C/min, Air): $T_{d10\%} = 370$ °C. Due to insolubility, no further characterization methods were used.

2-(4-Ethenylphenyl)-4,4,5,5-tetramethyl-1,3,2-dioxaborolane (styryl-B(pin), S3). The synthesis of **S3** was performed following a modified procedure by Speer et al.[15] *n*-BuLi (2.5 M in THF, 7.5 mL, 18.6 mmol) was added dropwise to a solution of 1-bromo-4-ethenylbenzene (2.2 mL, 16.9 mmol) in anhydrous THF (30 mL) at −78 °C. After stirring for 1 h, 2-isopropoxy-4,4,5,5-tetramethyl-1,3,2-dioxaborolane (3.5 mL, 18.6 mmol) was added dropwise to the solution. The solution was allowed to warm to room temperature and was stirred for an additional two hours. Saturated aq. NH_4Cl (10 mL) was added, and the organic layer was separated. The aqueous layer was extracted with diethyl ether (2×10 mL). The combined organic layers were washed with brine (5 mL), dried ($MgSO_4$), filtered, and the solvents were removed under vacuum. Column chromatography (silica gel, cyclohexane/EtOAc: 10/1) afforded **S3** (2.65 g, quant.) as a colorless oil. ^{1}H NMR (400 MHz, $CDCl_3$): δ 7.78–7.75 (m, 2H), 7.42–7.39 (m, 2H), 6.72 (dd, J = 17.7, 10.9 Hz, 1H), 5.80 (dd, J = 17.7, 1.0 Hz, 1H), 5.29 (dd, J = 10.9, 1.0 Hz, 1H), 1.34 (s, 12H); ^{13}C NMR (101 MHz, $CDCl_3$): δ 140.2, 136.9, 135.0, 127.8 (d, $^1J_{C,B}$ = 45.5 Hz), 125.5, 114.8, 83.7, 24.9; HRMS (ESI+): *m/z* calcd. for $C_{14}H_{23}BO_2N$ 248.1822 $[M+NH_4]^+$, found 248.1816.

10-(4-Methoxyphenyl)-3-(4-vinylphenyl)-10*H*-phenothiazine (3). 3,7-Dibromo-10-(4-methoxyphenyl)-10*H*-phenothiazine (**S2**; 300 mg, 0.65 mmol) was dissolved in anhydrous THF (8 mL) and cooled to −78 °C. *n*-BuLi (0.40 mL, 0.65 mmol) was added dropwise, and the mixture stirred for 30 min at −78 °C. MeOH (35 μL) was added, and the reaction stirred for another 30 min before allowing to warm up to room temperature. H_2O was added, and the aqueous layer was extracted with ethyl acetate (3×75 mL). The combined organic layers were washed with brine, dried over $MgSO_4$, filtered and evaporated to dryness and directly used without further purification. A mixture of **S3** (0.17 mL, 0.99 mmol) and $Pd(PPh_3)_4$ (15 mg, 13 μmol, 6 mol%) in a degassed mixture of THF (5 mL) and aq. NaOH (10 wt%, 1.2 mL) was heated to 90 °C for 4 h. The reaction was cooled to room temperature, H_2O was added, and the aqueous layer was extracted with dichloromethane (3×25 mL). The combined organic layers were dried over $MgSO_4$, filtered and evaporated to dryness under reduced pressure. Column chromatography (silica gel, cyclohexane/EtOAc: 50/1 to 20/1 + 5 mol% Et_3N) afforded **3** (225 mg, 0,55 mmol, 85%) as an orange solid. ^{1}H NMR (300 MHz, $CDCl_3$) δ 7.47–7.40 (m, 4H), 7.36–7.29 (m, 2H), 7.24 (d, J = 2.2 Hz, 1H), 7.16–7.10 (m, 2H), 7.06 (d, J = 8.6, 2.2 Hz, 1H), 7.02–6.98 (m, 1H), 6.87–6.75 (m, 2H), 6.73 (m, 1H), 6.23 (d, J = 8.6 Hz, 1H), 6.20 (m, 1H), 5.76 (dd, J = 17.6, 1,0 Hz, 1H), 5.24 (dd, J = 10.9, 0.9 Hz, 1H), 3.91 (s, 3H); ^{13}C NMR (101 MHz, $CDCl_3$) δ 159.4, 144.5, 143.7, 139.3, 136.5, 136.3, 134.8, 133.3, 132.2, 127.4, 127.0, 126.9, 126.8, 126.7, 126.4, 125.3, 124.9, 122.4, 120.2, 119.4, 116.1, 115.9, 115.8, 113.7, 55.6; HRMS (APCI+): *m/z* calcd. for $C_{27}H_{22}NOS$ 408.1422 $[M+H]^+$, found 408.1418.

Poly(10-(4-methoxyphenyl)-3-(4-vinylphenyl)-10H-phenothiazine) (PSAPT). A solution of AIBN (0.8 mg, 49 μmol) in anhydrous THF (0.1 mL) was added to a solution of 10-(4-methoxyphenyl)-3-(4-vinylphenyl)-10*H*-phenothiazine (**3**, 100 mg, 245 μmol) in THF, placed in a pre-heated oil bath and stirred at 70 °C for 15 h. The reaction was cooled to room temperature and MeOH was added. After evaporation, the residue was centrifugated in cyclohexane (5000 rpm, 5 min). The supernatant was removed, and further centrifugation with ethyl acetate, acetone and DCM was performed similarly (9000 rpm, 10 min). The supernatant was removed and the

precipitate evaporated to dryness to afford **PSAPT** (88 mg, 88%) as a yellow solid. TGA (10 °C/min, N_2): $T_{d10\%} = 366$ °C. Due to insolubility, no further characterization methods were used. This material was used for battery electrode measurements. Using 10 mol% AIBN, a slightly more soluble variant of **PSAPT** was prepared and used for the CV and UV/Vis spectroscopic measurements.

Poly(10-(4-methoxyphenyl)-3-(4-vinylphenyl)-10*H*-phenothiazine-*co*-divinylbenzene) (PSAPT-X-DVB). To a solution of 10-(4-methoxyphenyl)-3-(4-vinylphenyl)-10*H*-phenothiazine (**3**, 320 mg, 785 μmol) in THF (1 mL) were added AIBN (6 mg, 37 μmol, 5 mol%) and divinylbenzene (mixture of 1,3- and 1,4-isomer, 13 mg, 79 μmol, 10 mol%). The mixture was placed in a pre-heated oil bath at 70 °C and stirred for 17 h and cooled to room temperature afterwards. MeOH was added and the solvent was evaporated. The residue was purified by successive Soxhlet extraction with MeOH, ethyl acetate and CH_2Cl_2. The volatiles were removed under reduced pressure, and **PSAPT-X-DVB** (195 mg, 61%) was obtained as a yellow solid. TGA (10 °C/min, N_2): $T_{d10\%} = 396$ °C. Due to insolubility, no further characterization methods were used.

Acknowledgements

We thank Dr. Mathias Hermann and Dr. Jan Wössner for X-ray structural data resolution. This research was funded by the Deutsche Forschungsgemeinschaft (DFG, German Research Foundation), project numbers 230408635 and 398214985, and the state of Baden-Württemberg through bwHPC. This work contributes to the research performed at CELEST (Center for Electrochemical Energy Storage Ulm-Karlsruhe) and was funded by the German Research Foundation (DFG) under Project ID 390874152 (POLiS Cluster of Excellence, EXC 2154). Open Access funding enabled and organized by Projekt DEAL.

Conflict of Interest

The authors declare no conflict of interest.

Data Availability Statement

The data that support the findings of this study are available from the corresponding author upon reasonable request.

Keywords: π-π interactions · high rate capability · organic batteries · positive electrode materials · redox polymers

[1] P. Poizot, F. Dolhem, *Energy Environ. Sci.* **2011**, *4*, 2003–2019.
[2] S. Lee, J. Hong, K. Kang, *Adv. Energy Mater.* **2020**, *2*, 2001445.
[3] S. Dühnen, J. Betz, M. Kolek, R. Schmuch, M. Winter, T. Placke, *Small Methods* **2020**, *4*, 2000039.
[4] B. Esser, F. Dolhem, M. Becuwe, P. Poizot, A. Vlad, D. Brandell, *J. Power Sources* **2021**, *482*, 228814.
[5] P. Poizot, J. Gaubicher, S. Renault, L. Dubois, Y. Liang, Y. Yao, *Chem. Rev.* **2020**, *120*, 6490–6557.
[6] C. N. Gannett, L. Melecio-Zambrano, M. J. Theibault, B. M. Peterson, B. P. Fors, H. D. Abruña, *Mater. Reports Energy* **2021**, *1*, 100008.
[7] K. Shang, J. Gao, X. Yin, Y. Ding, Z. Wen, *Eur. J. Inorg. Chem.* **2021**, 606–619.
[8] M. D. Hager, B. Esser, X. Feng, W. Schuhmann, P. Theato, U. S. Schubert, *Adv. Mater.* **2020**, *32*, 2000587.
[9] B. Esser, *Org. Mater.* **2019**, *01*, 063–070.
[10] Y. Chen, C. Wang, *Acc. Chem. Res.* **2020**, *53*, 2636–2647.
[11] Y. Lu, Q. Zhang, L. Li, Z. Niu, J. Chen, *Chem* **2018**, *4*, 2786–2813.
[12] J. F. Mike, J. L. Lutkenhaus, *ACS Macro Lett.* **2013**, *2*, 839–844.
[13] P. Acker, M. E. Speer, J. S. Wössner, B. Esser, *J. Mater. Chem. A* **2020**, *8*, 11195–11201.
[14] G. Desmaizieres, M. E. Speer, I. Thiede, P. Gaiser, V. Perner, M. Kolek, P. Bieker, M. Winter, B. Esser, *Macromol. Rapid Commun.* **2021**, *42*, 2000725.
[15] M. E. Speer, C. Sterzenbach, B. Esser, *ChemPlusChem* **2017**, *82*, 1274–1281.
[16] F. Otteny, G. Desmaizieres, B. Esser, in *Redox Polym. Energy Nanomedicine* (Eds.: N. Casado, D. Mecerreyes), Royal Society Of Chemistry, **2020**, pp. 166–197.
[17] M. Rajesh, F. Dolhem, C. Davoisne, M. Becuwe, *ChemSusChem* **2020**, *13*, 2364–2370.
[18] X. Wang, G. Li, Y. Han, F. Wang, J. Chu, T. Cai, B. Wang, Z. Song, *ChemSusChem* **2021**, *14*, cssc.202101008.
[19] Y. Liu, Z. Niu, G. Dai, Y. Chen, H. Li, L. Huang, X. Zhang, Y. Xu, Y. Zhao, *Mater. Today Energy* **2021**, *21*, 100812.
[20] B. M. Peterson, L. Shen, G. J. Lopez, C. N. Gannett, D. Ren, H. D. Abruña, B. P. Fors, *Tetrahedron* **2019**, *75*, 4244–4249.
[21] B. M. Peterson, D. Ren, L. Shen, Y.-C. M. Wu, B. Ulgut, G. W. Coates, H. D. Abruña, B. P. Fors, *ACS Appl. Energ. Mater.* **2018**, *1*, 3560–3564.
[22] N. Casado, D. Mantione, D. Shanmukaraj, D. Mecerreyes, *ChemSusChem* **2020**, *13*, 2464–2470.
[23] L. Zhang, H. Wang, X. Zhang, Y. Tang, *Adv. Funct. Mater.* **2021**, *31*, 2010958.
[24] T. Placke, A. Heckmann, R. Schmuch, P. Meister, K. Beltrop, M. Winter, *Joule* **2018**, *2*, 2528–2550.
[25] P. Poizot, F. Dolhem, J. Gaubicher, *Curr. Opin. Electrochem.* **2018**, *9*, 70–80.
[26] P. Acker, J. S. Wössner, G. Desmaizieres, B. Esser, *ACS Sustainable Chem. Eng.* **2022**, *10*, 3236–3244.
[27] P. Acker, L. Rzesny, C. F. N. Marchiori, C. M. Araujo, B. Esser, *Adv. Funct. Mater.* **2019**, *29*, 1906436.
[28] M. Kolek, F. Otteny, P. Schmidt, C. Mück-Lichtenfeld, C. Einholz, J. Becking, E. Schleicher, M. Winter, P. M. Bieker, B. Esser, *Energy Environ. Sci.* **2017**, *10*, 2334–2341.
[29] C. Wang, *Energy Environ. Mater.* **2020**, *3*, 441–452.
[30] F. Otteny, V. Perner, D. Wassy, M. Kolek, P. Bieker, M. Winter, B. Esser, *ACS Sustainable Chem. Eng.* **2020**, *8*, 238–247.
[31] M. Kolek, F. Otteny, J. Becking, M. Winter, B. Esser, P. Bieker, *Chem. Mater.* **2018**, *30*, 6307–6317.
[32] F. Otteny, M. Kolek, J. Becking, M. Winter, P. Bieker, B. Esser, *Adv. Energy Mater.* **2018**, *8*, 1802151.
[33] V. Perner, D. Diddens, F. Otteny, V. Küpers, P. Bieker, B. Esser, M. Winter, M. Kolek, *ACS Appl. Mater. Interfaces* **2021**, *13*, 12442–12453.
[34] F. Otteny, G. Studer, M. Kolek, P. Bieker, M. Winter, B. Esser, *ChemSusChem* **2020**, *13*, 2232–2238.
[35] F. Otteny, V. Perner, C. Einholz, G. Desmaizieres, E. Schleicher, M. Kolek, P. Bieker, M. Winter, B. Esser, *ACS Appl. Energ. Mater.* **2021**, *4*, 7622–7631.
[36] J. Lv, J. Ye, G. Dai, Z. Niu, Y. Sun, X. Zhang, Y. Zhao, *J. Energy Chem.* **2020**, *47*, 256–262.
[37] F. A. Obrezkov, A. I. Somova, E. S. Fedina, S. G. Vasil'ev, K. J. Stevenson, P. A. Troshin, *Energy Technol.* **2021**, *9*, 2000772.
[38] L. Mayer, L. May, T. J. J. Müller, *Org. Chem. Front.* **2020**, *7*, 1206–1217.
[39] All capacities herein are reported per mass of active material.
[40] I. Cekic-Laskovic, N. von Aspern, L. Imholt, S. Kaymaksiz, K. Oldiges, B. R. Rad, M. Winter, *Top. Curr. Chem.* **2017**, *375*, 37.
[41] SAINT V8.37A, Bruker AXS, Madison, Wisconsin, USA, 2015.

Manuscript received: October 24, 2022
Revised manuscript received: December 1, 2022
Accepted manuscript online: December 8, 2022
Version of record online: December 29, 2022